




First-principles study of electronic and diffusion properties of intrinsic defects in 4H-SiC

Cite as: J. Appl. Phys. 127, 085702 (2020); doi: 10.1063/1.5140692

Submitted: 2 December 2019 · Accepted: 7 February 2020 ·

Published Online: 24 February 2020



Xiaolan Yan,  Pei Li, Lei Kang, Su-Huai Wei,  and Bing Huang 

AFFILIATIONS

Beijing Computational Science Research Center, Beijing 100193, China

Note: This paper is part of the Special Topic on Defects in Semiconductors 2020.

^{a)}Authors to whom correspondence should be addressed: bing.huang@csrc.ac.cn and suhuaiwei@csrc.ac.cn

ABSTRACT

As a wide bandgap semiconductor, SiC holds great importance for high temperature and high power devices. It is known that the intrinsic defects play key roles in determining the overall electronic properties of semiconductors; however, a comprehensive understanding of the intrinsic defect properties in the prototype 4H-SiC is still lacking. In this study, we have systematically investigated the electronic properties and kinetic behaviors of intrinsic point defects and defect complexes in 4H-SiC using advanced hybrid functional calculations. Our results show that all the point defects in 4H-SiC have relatively high formation energies, i.e., low defect concentrations even at high growth temperatures. Interestingly, it is found that the migration barriers are very high for vacancies (>3 eV) but relatively low for interstitial defects (~ 1 eV) in SiC. Meanwhile, the diffusion energy barriers of defects strongly depend on their charge states due to the charge-state-dependent local environments. Furthermore, we find that V_{Si} in SiC, a key defect for quantum spin manipulation, is unstable compared to the spin-unpolarized V_C-C_{Si} complex in terms of the total energy (under p -type conditions). Fortunately, the transformation barrier from V_{Si} to V_C-C_{Si} is as high as 4 eV, which indicates that V_{Si} could be stable at room (or not very high) temperature.

Published under license by AIP Publishing. <https://doi.org/10.1063/1.5140692>

I. INTRODUCTION

Silicon carbide (SiC) is widely considered as an alternative to silicon (Si) in the high temperature and high-voltage power devices because of its unique physical properties, i.e., wide bandgap, high breakdown electric field strength, and high thermal conductivity.^{1,2} The breakdown field strength of SiC is about ten times higher than that of Si, enabling the SiC devices to be much thinner with lower conduction and switching loss. Due to its high thermal conductivity, SiC has been widely used in high temperature and high power device applications.^{3–5} Because of its wide bandgap and radiation hardness, the performance of SiC devices can maintain good stability even under strong irradiation environments.^{6–8} In addition, it has been proposed that Si vacancy (V_{Si}) can be used as a quantum bit because its spin states can be manipulated for quantum computing at room temperature.^{9–11}

The understanding of the intrinsic defect properties in SiC, which play a critical role in determining its overall electric properties, is of great importance for the development of SiC-based electronic devices. Among its various allotropes, 4H-SiC is widely adopted in high-power devices, due to its high electron mobility

and availability of high-quality epitaxial wafers.^{1,4} The major intrinsic defects that largely deteriorate the electronic properties of 4H-SiC are labeled as $Z_{1/2}$ ¹² and $EH_{6/7}$,¹³ which are generally found in epitaxial 4H-SiC.^{14–18} The defect levels of $Z_{1/2}$ and $EH_{6/7}$ are located at 0.5–0.7 eV and 1.5–1.6 eV below the conduction band minimum (CBM), respectively, as detected by the deep-level transient spectroscopy (DLTS).^{19,20} Since it is difficult to directly identify the defect types for $Z_{1/2}$ and $EH_{6/7}$ in the experiments, the extensive theoretical calculations have been carried out for this purpose, e.g., some calculations suggest that carbon vacancy defects are the main sources for the $Z_{1/2}$ and $EH_{6/7}$ levels.^{21–25}

The intrinsic defects in 3C-SiC, including vacancies, antisites, and interstitials, have been studied using local-density approximation (LDA) calculations.^{26–28} Meanwhile, several point defects, e.g., vacancies and divacancies, have also been investigated in 4H- and 6H-SiC.^{29,30} However, it is well-known that LDA-level calculations could seriously underestimate the bandgap of semiconductors, which may make their calculated defect properties unreliable. Although the defect properties of vacancies in 3C- and 4H-SiC have also been investigated using Hyde-Scuseria-Ernzerhof (HSE)

hybrid functional^{31,32} with corrected bandgap,^{21,33} a systematic understanding of all the intrinsic defects in 4H-SiC, including their diffusion properties using HSE functional, is still lacking, which is the main purpose of our study.

In this study, the advanced HSE06 hybrid functional is adopted to calculate intrinsic defect properties in 4H-SiC. Our results show that all the point defects in intrinsic 4H-SiC have high formation energies, which correspond to the low defect concentrations at thermal equilibrium growth conditions. Meanwhile, we find that the vacancies have high migration barriers (~ 3 eV), whereas the interstitial defects have low energy barriers (~ 1 eV) in SiC. Interestingly, the diffusion barriers of defects could also strongly depend on their charge states, which is mainly due to the different local distortion around the defects at different charge states. Furthermore, we find that V_{Si} is unstable because it can convert to the V_C-C_{Si} complex with a lower total energy under p -type conditions. Fortunately, the transformation barrier from V_{Si} to V_C-C_{Si} is ~ 4 eV, which indicates that V_{Si} could be stable at room (or not very high) temperature.

II. METHODOLOGY

A. Computational details

All the calculations were carried out using the Vienna Ab initio Simulation Package (VASP).³⁴ The exchange-correlation energy was treated both with the generalized gradient approximation (GGA) in the Perdew–Burke–Ernzerhof (PBE) form³⁵ and with the screened HSE06 hybrid density functional.^{31,32} The plane-wave cutoff for the wavefunction expansion was set to 400 eV. Sufficiently, k -points were selected to make the total energies of calculated systems converged. During the structural relaxations, a conjugate-gradient algorithm was used until the force on each atom was lower than $0.01 \text{ eV } \text{\AA}^{-1}$, and the total energy was converged to $1.0 \times 10^{-5} \text{ eV}$. The spin-polarized calculations were considered for all the defects in 4H-SiC. For the $4 \times 4 \times 1$ supercell (128 atoms), a $2 \times 2 \times 2$ Monkhorst-Pack k -point mesh for integrations over the Brillouin zone are used in the calculations. The calculated lattice parameters are $a = 3.07 \text{ \AA}$, $c = 10.05 \text{ \AA}$, and the calculated bandgap is 3.19 eV in the HSE06 calculation, in good agreement with available experimental results.¹

The single defect levels are obtained by comparing the defect levels in defect cells and the VBM (valence band maximum) in the perfect cells according to aligned core levels of atoms furthest away from the defect center in defect cells to that of the perfect cells. The single- k -point calculations were performed to determine the defect levels. For the calculations of migration barrier, the CI-NEB methods, an effective method for finding the saddle points and minimum energy paths between initial and final states,³⁶ are adopted. The total energy and the force on each atom were converged to $< 1.0 \times 10^{-5} \text{ eV}$ and $< 0.02 \text{ eV } \text{\AA}^{-1}$, respectively. The number of images depends on the distance of the diffusion path between initial and final states, the distance between each image is not less than 0.8 \AA .

B. Formation energies of defects

The formation energy (E^f) of a defect can be evaluated as³⁷

$$E^f(\alpha, q) = \Delta E(\alpha, q) + \sum_i n_i \mu_i + qE_F + \Delta E_{\text{align}}(\alpha, q), \quad (1)$$

where $\Delta E(\alpha, q) = E(\alpha, q) - E(\text{host}) + \sum_i n_i E_i + qE_V$. $E(\text{host})$ is the total energy of the supercell without a defect, and $E(\alpha, q)$ is the total energy of a supercell with a defect in a charge state q . q is the number of electrons transferred from the supercell to the reservoirs in forming the defect cell and n_i is the number of atoms removed from or added into the supercell, E_i is the total energy of C or Si at its ground state, and μ_i is the chemical potential of atom i with respect to E_i . In this work, two limiting chemical potential conditions were considered, i.e., C-rich and Si-rich. Meanwhile, μ_{Si} and μ_C are limited by the formation energy of bulk SiC. That is, the maximum value of μ_C (under C-rich condition) is given by bulk diamond (defined as zero), while the minimum value of μ_C (under C-poor condition) is the formation energy of SiC. E_V and E_F are the energy of valence band maximum (VBM) and the Fermi level with respect to VBM, respectively. $\Delta E_{\text{align}}(\alpha, q)$ is determined by aligning the core levels of atoms furthest away from the defect center in defect cells to that of the perfect cells.

We also examine the charge-state transition levels (CTLs), which are defined as

$$\varepsilon(q_1/q_2) = \frac{(E(\alpha, q_1) + \Delta E_{\text{align}}(\alpha, q_1)) - (E(\alpha, q_2) + \Delta E_{\text{align}}(\alpha, q_2))}{q_2 - q_1} - E_V. \quad (2)$$

C. Concentrations of defects

Under thermodynamic equilibrium condition, the concentration of defects obeys the Boltzmann distribution that is related to their formation energies E^f ,³⁸

$$C = N_{\text{sites}} g_q \exp(-E^f(\alpha, q)/k_B T). \quad (3)$$

Here, N_{sites} is the number of sites that defects can be incorporated per volume, k_B is Boltzmann's constant, T is the temperature, and g_q is the degeneracy factor that equals to the number of possible electron configurations for different charge states. With the constraint of charge neutrality condition,

$$p_0 + N_D^+ = n_0 + N_A^-, \quad (4)$$

where p_0 and n_0 are the concentrations of thermally excited holes and electrons, N_D^+ and N_A^- are the total concentrations of positive and negative charge induced by defects, respectively. The defect concentrations c and the Fermi energy level E_F can be calculated self-consistently as a function of T and the growth chemical potentials μ_i .

At a given temperature, the p_0 and n_0 in Eq. (4) are determined by

$$p_0 = N v e^{-(E_F - E_V)/k_B T} = N v e^{-E_F/k_B T}, \quad N_V = 2 \frac{(2\pi m_p^* k_B T)^{3/2}}{h^3}, \quad (5)$$

$$n_0 = N_C e^{-(E_C - E_F)/k_B T} = N_C e^{(E_F - E_g)/k_B T}, \quad N_C = 2 \frac{(2\pi m_n^* k_B T)^{3/2}}{h^3}, \quad (6)$$

where E_V and E_C are VBM and CBM energies, and E_V generally set to 0, while $E_C = E_g$ (E_g is the bandgap). N_V and N_C are the effective density of states (DOS) of the valence band and the conduction band, m_p^* and m_n^* are the effective mass of hole and electron, respectively.

In practice, quenching is often used to improve the defect property, in which the 4H-SiC can be grown under various high temperatures but quenched to room temperature. Therefore, we also calculate the defect concentrations under growth temperature (GT), and then quenching it to room temperature, keeping the sum of the defect densities fixed and recalculating the density of the charged defects at room temperature (RT). In this situation, the equilibrium E_F and carrier densities are changed before and after quenching.

III. RESULTS AND DISCUSSION

The 4H-SiC has two inequivalent sites for C and Si, i.e., cubic sites (k) and hexagonal sites (h), as shown in Fig. 1. Our test calculations indicate that the defect states have similar characters at these two different sites (the detailed defect structures are shown as Fig. S1 in the supplemental material). For an ideal C vacancy (V_C) or Si vacancy (V_{Si}) defect, the remaining four dangling bonds located at the surrounding Si (C) atom sites give rise to two single a_1 states and a double-degenerated e states, which is induced by the local crystal field splitting of C_{3v} symmetry. After the structural relaxation, the local symmetry around a vacancy will be reduced from C_{3v} to C_{1h} , which leads to the a_1 states appearing as a' states and the e states splitting to a' and a'' states. Our calculations confirm that the ground state of a V_C defect prefers a low-spin configuration, while V_{Si} prefers a high-spin state, as shown in Fig. 2. This difference is mainly caused by the difference of exchange interactions of the delocalized $3p$ electrons of Si around a V_C and localized $2p$ electrons of C atom around a V_{Si} . The defect levels of V_C , derived from its nearest neighbor Si

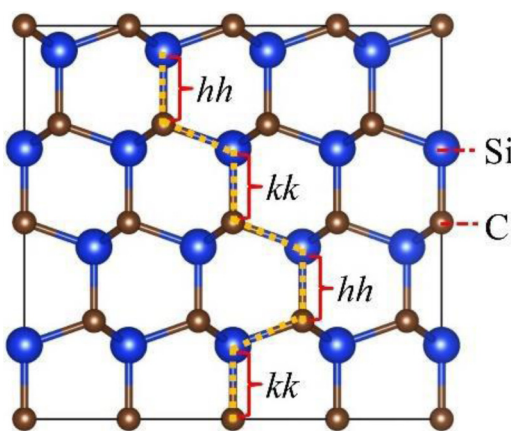


FIG. 1. Supercell structure of 4H-SiC used for defect calculations. Blue and brown balls indicate the Si and C atoms, respectively. There are two inequivalent lattice sites, named as h -site and k -site.

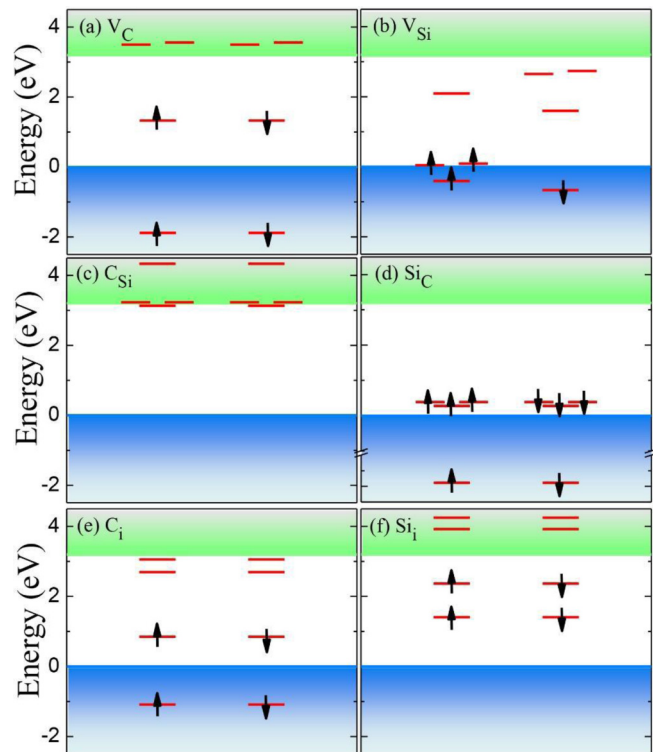


FIG. 2. Single-particle defect levels for the intrinsic defects at k -sites in 4H-SiC for (a) V_C , (b) V_{Si} , (c) C_{Si} , (d) Si_C , (e) C_i , and (f) Si_i . See text for the detailed explanations. Green and blue regions indicate the conduction band (CB) and the valence band (VB), respectively. The up and down arrows denote the occupied spin-states of electrons on the defect levels.

dangling bonds, lie closer to the CBM than that of V_{Si} [Figs. 2(a) and 2(b)]. For the cases of isovalent antisite defects, i.e., C on Si (C_{Si}) and Si on C (Si_C), their defect levels in the gap are fully empty [Fig. 2(c)] or occupied [Fig. 2(d)]. For the interstitial defects, i.e., C interstitials (C_i), as shown in Fig. 2(e), one of the defect levels in the bandgap is occupied by two electrons while the other one is empty, which means that the C_i defect may further behave as -2 or $+2$ charge states when the E_F position is changed inside the bandgap. On the other hand, the empty Si_i defect levels are above the CBM, so they may only exhibit positive charge states.

We have also calculated the E^f and CTLs for these defects, as shown in Fig. 3. For each defect, there is a stable charge state with the lowest energy at each value of E_F (Fig. 3), i.e., once the E_F of the system is given, the stable charge states of all the defects can be obtained. The slope in Fig. 3 represents the charge state, and the vertices represent the CTLs between two different charge states. Interestingly, it is noted that the CTLs of defects at the h -site and k -site are different, even if they have a similar E^f at neutral states, except for the interstitial defects. Generally, the E^f of Si-related defects are higher than that of C-related defects. On the neutral charge state, the

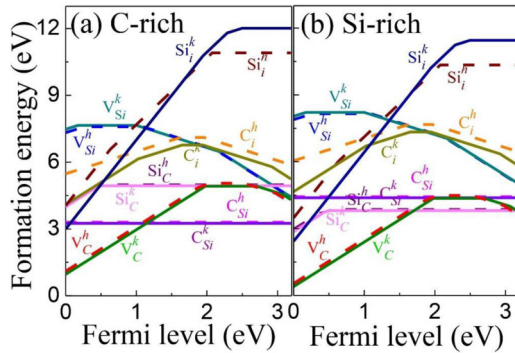


FIG. 3. Formation energies of intrinsic defects under (a) C-rich and (b) Si-rich chemical conditions. Solid and dashed lines indicate the defects located at k -sites and h -sites, respectively. Zero of Fermi level is set to the position of VBM.

antisite C_{Si} has a lower energy than Si_C defects because it is easier to substitute a small-size atom at a large-size atom site. Although the E_f of C_{Si} is lower in a large range of E_F , its defect level is resonated in the valence band. On the other hand, although the interstitial defects (Si_i and C_i) have relatively high E_f , they still could be formed in a positive charge states under p -type growth conditions. The positively-charged and negatively-charged V_C become more favorable under p -type and n -type

growth conditions respectively, while negatively-charged V_{Si} is favorable under n -type growth conditions. Interestingly, the donor level of V_C is found to exhibit a negative- U behavior at the k -site. The 0/−1 CTLs of V_C is located around $E_C - (0.5 - 0.7)$, which is close to the position of $Z_{1,2}$ observed in the experiments. Therefore, the V_C could be the most important defect that can downgrade the electronic properties of SiC during device applications.

After obtaining the E_f and CTLs of the intrinsic defects in 4H-SiC, we can estimate their defect concentrations at a given GT, while the working temperature is set to RT. SiC is generally grown at a high temperature, e.g., the common GT is 1850 K.¹ As can be seen in Fig. 4(a), the calculated E_F is located near the middle of the bandgap. This is because band-edge excitation dominates at this temperature, even though more intrinsic defects can be created when GT increases. When quenched to RT, the total concentration of all the defects is assumed fixed at that created at GT, but the concentrations of defects at different charge states can be redistributed. At RT, the thermally excited electrons and holes are significantly reduced. The amount of positively charged V_C induced electrons moves the E_F toward the CBM. The E_f of C_{Si} and Si_C are independent of the E_F . However, when E_F moves toward the CBM, V_C prefers to form negative charge states and the concentration of the negatively charged V_C increases. When the temperature quenched from 1850 K to 300 K, the defect concentration of V_C is about 10^{12} cm^{-3} under Si-rich condition, which is generally consistent with the experimental results.¹

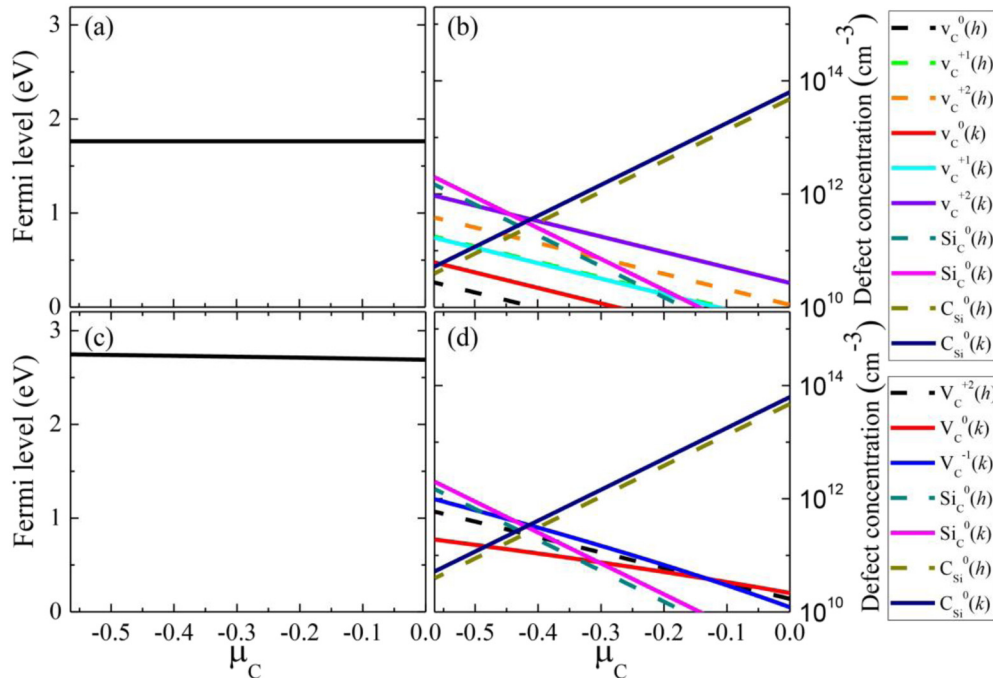


FIG. 4. Fermi energy E_F (left panel) and defect concentration (right panel) of intrinsic defects before: (a) and (b) and after: (c) and (d) quenching. Growth temperature is set to 1850 K, while working temperature is set to room temperature. Solid and dashed lines indicate the defects located at k -sites and h -sites, respectively.

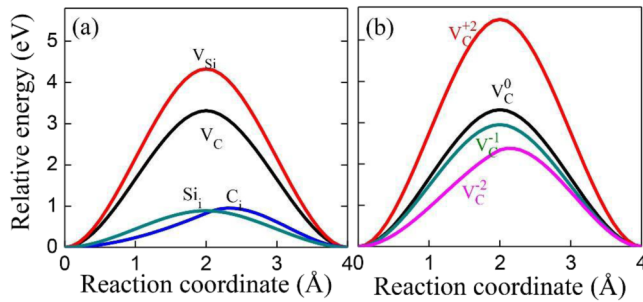


FIG. 5. (a) Diffusion barriers of various intrinsic defects in 4H-SiC; (b) diffusion barriers of V_C at different stable charge states. It is noted that the intermediate image structures for these defects along the reaction coordinates can be found in Fig. S2 in the [supplementary material](#).

Overall, the concentrations of all intrinsic defects in intrinsic 4H-SiC are relatively low.

In the experiments, the annealing process is necessary after the growth of 4H-SiC in order to reduce the native defect concentrations and improve its electronic properties.^{14,18} During the annealing process, the defects can be reactivated and diffused. Therefore, it is also important to understand the diffusive properties of defects in 4H-SiC. In order to investigate the diffusion path of intrinsic defects, the CI-NEB methods³⁶ are used, and the results are shown in Fig. 5. It is found that the diffusion barriers of antisite defects are extremely high (~ 10 eV, not shown in Fig. 5), as the diffusion of C and Si simultaneously could give rise to the large local structural distortions (corresponding to high strain energies). For isolated vacancies, their diffusion barriers are also very large, i.e., 3.3 eV for V_C and 4.3 eV for V_{Si} . On the other hand, it is found that the interstitial defects have relatively low energy barriers, i.e., 0.95 eV for C_i and 0.88 eV for Si_i , which indicates that they could diffuse fast during the annealing process at high temperature. The intermediate image structures for these defects along the reaction coordinates can be found in Fig. S2 in the [supplementary material](#).

Interestingly, it is also found that the charge states of a defect can strongly affect its diffusion barrier. Taking V_C as a typical example, we have calculated the diffusion barriers of V_C at different possible charge states, as shown in Fig. 5(b). Interestingly, the calculated diffusion barriers of V_C gradually increase as its charge states change from negative to positive ones, which is accompanied by a large outward atomic relaxation effects around the defect sites. Therefore, the structural changes caused by the different electron occupations of V_C are the major reason for the charge-state-dependent diffusion barrier. Similarly, the migration barriers for V_{Si} and interstitials also exhibit charge-state-dependent behaviors, as shown in Fig. S3 in the [supplementary material](#).

Besides the single point defects, the defect complexes could also exist in 4H-SiC, e.g., antisite-vacancy pair (V_C - C_{Si}) and divacancy (V_C - V_{Si}) are two typical examples. In practice, V_C - C_{Si} may also be transformed from V_{Si} , as the E_f^f of V_C - C_{Si} under the neutral state is ~ 0.6 eV lower than that of V_{Si} , as shown in Fig. 6(a). According to the charge state calculations, V_C - C_{Si} is more stable under p -type condition but V_{Si} is more stable under n -type condition. The ground-state of V_C - C_{Si} is spin unpolarized, which is different from that of single V_{Si} . Therefore, the transformation from high-energy V_{Si} to low-energy V_C - C_{Si} under p -type condition could fundamentally eliminate the NV-center-like function of V_{Si} . However, the calculated energy diffusion barrier between the V_C - C_{Si} and V_{Si} is ~ 4 eV as shown in Fig. 6(b), indicating that V_{Si} still maybe stable at room-temperature once it can be formed.

For a V_C - V_{Si} divacancy, there are four inequivalent structures. As shown in Fig. 7, V_C - V_{Si} always exhibits high-spin configurations independent of its different local structures. The defect levels of V_C - V_{Si} can be understood as a combination of individual V_C and V_{Si} . In the cases of kk - and hh -divacancy structures, the degenerated e states originated from V_C and V_{Si} can maintain. While for kh - and hk -divacancy, the e states will be split to a' and a'' states. The E_f^f of V_C - V_{Si} is around 8.2 eV, which is independent of the chemical potentials. As shown in Fig. 6(c), the calculated diffusion barrier of V_C - V_{Si} divacancy is as high as ~ 4.5 eV.

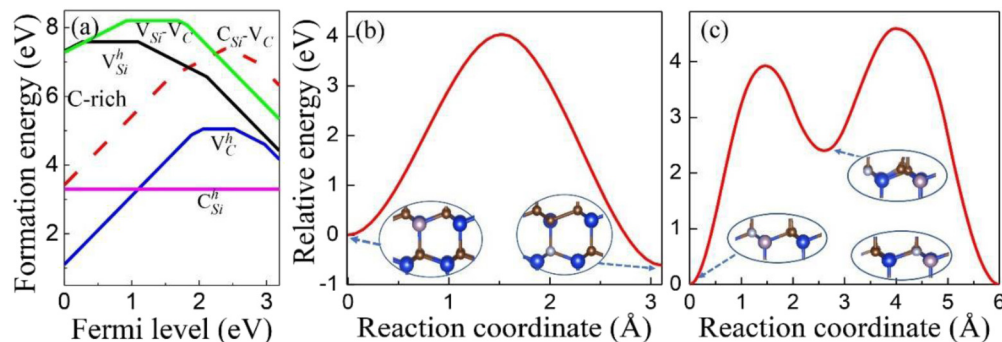


FIG. 6 (a) Formation energies of V_C - C_{Si} and V_C - V_{Si} defect complexes compared with single point defects under C-rich condition; (b) calculated diffusion barrier between V_{Si} and V_C - C_{Si} ; and (c) calculated diffusion barrier for the V_C - V_{Si} . Pink and gray balls indicate the Si and C vacancies, respectively.

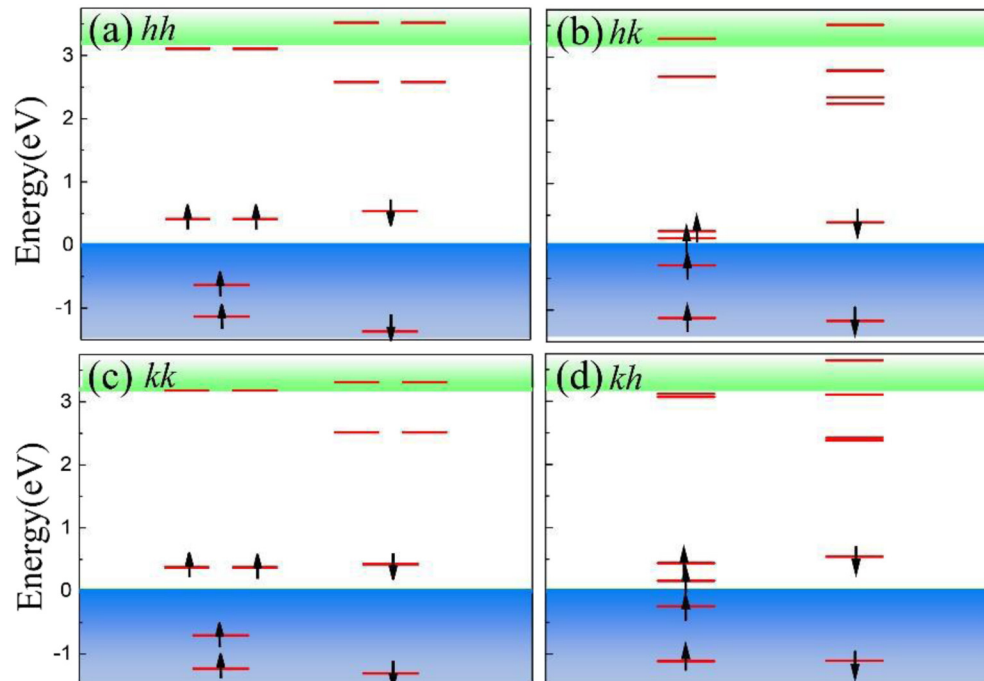


FIG. 7 Single-particle defect levels of four different types of V_C-V_{Si} in 4H-SiC: (a) hh combination; (b) hk combination; (c) kk combination; and (d) kh combination. Green and blue region indicate the conduction band (CB) and the valence band (VB) regions, respectively. The up and down arrows denote the occupied spin-states of electrons.

IV. CONCLUSION

The electronic and kinetic properties of intrinsic point defects and defect complexes in 4H-SiC have been systematically studied using advanced hybrid functional calculations. Among all the defects, antisite defects (C_{Si} and Si_C) and V_C have relatively lower formation energies than other defects. Since the defect levels of antisite defects are electronically inactive, the dominant harmful defect in 4H-SiC could be a deep-level V_C defect. For the point defects, the diffusion barriers of interstitial defects are <1 eV, while all the others are >3 eV, indicating that the interstitial defects could diffuse very fast in the annealing process. Interestingly, the diffusion barriers of defects in 4H-SiC can strongly depend on their charge states. In addition, the V_C-C_{Si} complex is found to have lower formation energy than that of V_{Si} at the neutral charge state, but the energy barrier for the formation of this defect complex is as high as 4 eV.

SUPPLEMENTARY MATERIAL

Local defect configurations of all the intrinsic defects, the image structures along the migration paths for V_C , V_{Si} , C_i , and Si_i , and diffusion energy barriers of V_{Si} , C_i , and Si_i at stable charge states are shown in the [supplementary material](#).

ACKNOWLEDGMENTS

This work is supported by the Science Challenge Project under No. TZ2016003 and NSFC Program under Grant Nos.

51672023 and 11634003, and NSAF Program under Grant No. U1930402. All the computations were performed at Tianhe2-JK at CSRC.

REFERENCES

1. T. Kimoto and J. A. Cooper, *Fundamentals of Silicon Carbide Technology: Growth, Characterization, Devices and Applications* (Wiley-IEEE Press, 2014).
2. F. Wang and Z. Zhang, *CPSS Trans. Power Electron. Appl.* **1**, 13 (2016).
3. T. Kimoto, *Jpn. J. Appl. Phys.* **54**, 040103 (2015).
4. J. A. Cooper and A. Agarwal, *Proc. IEEE* **90**, 956 (2002).
5. F. Roccaforte, P. Fiorenza, G. Greco, R. Lo Nigro, F. Giannazzo, F. Iucolano, and M. Saggio, *Microelectron. Eng.* **187-188**, 66 (2018).
6. A. A. Lebedev and V. V. Kozlovski, *Semiconductors* **48**, 1293 (2014).
7. M. Usman, A. Hallén, K. Gulbinas, and V. Grivickas, *Mater. Sci. Forum* **717-720**, 805 (2012).
8. V. V. Emtsev, A. M. Ivanov, V. V. Kozlovskii, A. A. Lebedev, G. A. Oganessian, and N. B. Strokan, *Semiconductors* **44**, 678 (2010).
9. R. Weber, W. F. Koehl, J. B. Varley, A. Janotti, B. B. Buckley, C. G. Van de Walle, and D. D. Awschalom, *J. Appl. Phys.* **109**, 102417 (2011).
10. P. G. Baranov, S. B. Orlinskii, and I. V. Borovykh, *Phys. Rev. B Condens. Matter* **83**, 125203 (2011).
11. D. Riedel *et al.*, *Phys. Rev. Lett.* **109**, 226402 (2012).
12. C. G. Hemmingsson, N. T. Son, A. Ellison, J. Zhang, and E. Janzén, *Phys. Rev. B* **58**, R10119 (1998).
13. C. G. Hemmingsson, N. T. Son, O. Kordina, J. P. Bergman, E. Janzén, J. L. Lindström, S. Savage, and N. Nordell, *J. Appl. Phys.* **81**, 6155 (1997).
14. Y. Negoro, T. Kimoto, and H. Matsunami, *Appl. Phys. Lett.* **85**, 1716 (2004).

- ¹⁵I. Pintilie, L. Pintilie, K. Irscher, and B. Thomas, *Appl. Phys. Lett.* **81**, 4841 (2002).
- ¹⁶J. Zhang, L. Storasta, J. P. Bergman, N. T. Son, and E. Janzén, *J. Appl. Phys.* **93**, 4708 (2003).
- ¹⁷K. Danno, T. Hori, and T. Kimoto, *J. Appl. Phys.* **101**, 053709 (2007).
- ¹⁸L. Storasta, H. Tsuchida, T. Miyazawa, and T. Ohshima, *J. Appl. Phys.* **103**, 013705 (2008).
- ¹⁹T. Kimoto *et al.*, *Appl. Phys. Lett.* **67**, 2833 (1995).
- ²⁰K. Danno and T. Kimoto, *J. Appl. Phys.* **100**, 113728 (2006).
- ²¹T. Hornos, A. Gali, and B. G. Svensson, *Mater. Sci. Forum* **679-680**, 261 (2011).
- ²²K. Szász, V. Ivády, I. A. Abrikosov, E. Janzén, M. Bockstedte, and A. Gali, *Phys. Rev. B* **91**, 121201 (2015).
- ²³J.-I. Iwata, C. Shinei, and A. Oshiyama, *Phys. Rev. B* **93**, 125202 (2016).
- ²⁴J. Coutinho, V. J. B. Torres, K. Demmouche, and S. Öberg, *Phys. Rev. B* **96**, 174105 (2017).
- ²⁵T. Kobayashi, K. Harada, Y. Kumagai, F. Oba, and Y.-i. Matsushita, *J. Appl. Phys.* **125**, 125701 (2019).
- ²⁶M. Bockstedte, A. Mattausch, and O. Pankratov, *Phys. Rev. B* **68**, 205201 (2003).
- ²⁷A. Zywietz, J. Furthmüller, and F. Bechstedt, *Phys. Rev. B* **62**, 6854 (2000).
- ²⁸A. Zywietz, J. Furthmüller, and F. Bechstedt, *Phys. Rev. B* **59**, 15166 (1999).
- ²⁹L. Torpo, M. Marlo, T. E. M. Staab, and R. M. Nieminen, *J. Phys. Condens. Matter* **13**, 6203 (2001).
- ³⁰J. Wiktor, G. Jomard, and M. Bertolus, *Nucl. Instrum. Methods Phys. Res. Sect. B* **327**, 63 (2014).
- ³¹J. Heyd and G. E. Scuseria, *J. Chem. Phys.* **118**, 8207 (2003).
- ³²J. Paier, M. Marsman, K. Hummer, G. Kresse, I. C. Gerber, and J. G. Angyán, *J. Chem. Phys.* **124**, 154709 (2006).
- ³³A. Csóré and Á. Gali, *Mater. Sci. Forum* **897**, 269 (2017).
- ³⁴G. Kresse and J. Furthmüller, *Phys. Rev. B Condens Matter* **54**, 11169 (1996).
- ³⁵J. P. Perdew, K. Burke, and M. Ernzerhof, *Phys. Rev. Lett.* **77**, 3865 (1996).
- ³⁶G. Henkelman, B. P. Uberuaga, and H. Jónsson, *J. Chem. Phys.* **113**, 9901 (2000).
- ³⁷S.-H. Wei, *Comput. Mater. Sci.* **30**, 337 (2004).
- ³⁸J. Ma, S.-H. Wei, T. A. Gessert, and K. K. Chin, *Phys. Rev. B* **83**, 245207 (2011).